

1 Anna Maria Ferrero⁽¹⁾, Maria Migliazza⁽²⁾, Marina Pirulli⁽³⁾

2

3

4 **Advance survey and modeling technologies for the study of the slope**
5 **stability in an Alpine basin**

6

7

8

9

10 ⁽¹⁾ Department of Earth Sciences, Università di Torino, Torino, Italy.

11 ⁽²⁾ Department of Earth Sciences “A. Desio”, Università degli Studi di Milano, Milano, Italy.

12 ⁽³⁾ Department of Structural, Geotechnical and Building Engineering, Politecnico di Torino, Torino, Italy.

13

14

15

16

17

18 Corresponding Author:

19

20 Marina Pirulli

21 Department of Structural, Geotechnical and Building Engineering, Politecnico di Torino,

22 Corso Duca degli Abruzzi, 24, 10129 Torino, ITALY.

23 Tel: +39 011 564 4865

24 Fax: +39 011 564 4899

25 Email: marina.pirulli@polito.it

26

1 **Abstract**

2

3 Alpine basins are typically characterized by an amphitheater shape with steep rocky walls on the
4 upper, a deposition zone of glacial debris in the middle and a channel in the lower part.

5 All different parts are in constant evolution and different kinds of instability phenomena can be
6 identified: rock fall at the top rocky walls, rotational sliding of the deposit and debris flow in the
7 channel down the valley. The different kinds of instability are somehow connected among them since
8 the rock fall can power the rock debris that can trigger a debris flow.

9 All different phenomena are chained in a global basin evolution also connected with seasonal climate
10 variation that can induce different water presence and different water phase (liquid/solid). Moreover
11 instability phenomena seem to increase in frequencies and magnitudes in the latest decades possibly
12 connected to climate change.

13 This paper reports a study of the stability condition of an Alpine Basin in North-West Italy by applying
14 advance survey and modeling techniques: aerial photogrammetric survey of the rock wall, limit
15 equilibrium methods that take ice presence into account and finally numerical analysis of the debris
16 evolution along the slope. Parametric analyses aimed to quantify the influence of the different most
17 important aspects have also been carried on.

18 The application of advanced tools helped to better understand the study area failure and evolution
19 mechanisms and to identify some main points to investigate in detail.

20

21 **Keywords:** slope stability; hazard; permafrost; numerical simulation; debris flows

22

23

1 **1. INTRODUCTION**

2 During the last decades an increase in frequency and intensity of rock-fall and debris-flow events has been recorded
3 throughout the Alps (Ravanel and Deline, 2011; Censic, 2009, Ferrero et al., 2014), probably as a consequence of
4 permafrost degradation due to recent climate changes. The progressive growth of socio-economic activities in alpine areas
5 (e.g. tourism) could also make the situation worse, by increasing the risks related to the above mentioned natural events
6 (Jomelli et al., 2007). As a consequence, the need of taking into account the role of permafrost in high mountains hazard
7 assessment cannot be ignored.

8 At this regard, the awareness of alpine European countries of the problem was in particular raised in summer 2003, when
9 an exceptional heat wave hit central Europe and was accompanied by a large series of rock-fall events along the entire
10 alpine chain (Gruber et al., 2004). In consideration of the supranational character of climate warming and of related
11 impacts, the Alcotra 2007-2013 "RiskNat" strategic project, which is one of the EU-funded programs for helping cross-
12 border Europe's regions form partnerships to develop new solutions to economic, social and environmental challenges,
13 was promoted. The project aimed to create an interregional platform to exchange experiences and to develop new
14 methodologies that allow to bypass the difficulties due to environmental conditions of high mountain territories.

15 The here presented methodology was in particular elaborated in the frame of the activities B1-C1 "Hazards deriving from
16 high mountain environment evolution" of the above project, which were devoted to define procedures able to quantify
17 hazard due to permafrost evolution and to manage both the resulting risk and the interaction with existing structures.
18 Although this study has been developed in an Alpine basin it could apply to any mountain site similar by the morphological
19 point of view so also on the Rockies or on the Himalayas.

20 While recent progress in measurement technologies and modeling has significantly improved our understanding of the
21 relationship between permafrost and rock face stability (e.g. Harris et al., 2009), the identification of the role of permafrost
22 and in particular of permafrost degradation to the probability of occurrence and the intensity of debris flows is still lacking
23 of completeness (Rebetz et al., 1997; Zimmermann et al., 1997; Jomelli et al., 2004; Jomelli et al., 2007; Sattler et al.,
24 2008; Schoeneich et al., 2011).

25 Debris flows are made up of soil, rock, and water. Their flow characteristics depend on the dynamic interaction between
26 solid and fluid phases during propagation and are a function of the weight of each of the above mentioned phases. Common
27 dangerous characteristics of this type of events are represented by the quite total absence of premonitory signs, their high
28 velocities and long travel distances.

29 In general, the increase of air temperatures is affecting the hydraulic and geotechnical properties of perennially frozen
30 debris cones or slopes. But, the reaction of ground ice in sediment and scree slopes is only indirect and supposed to a time-
31 lag. It depends on the topographical conditions, on the structure of the surface and of the soil material, on the interaction
32 with the snow cover or avalanche deposits and on the ice content itself (Zischg et al., 2011). High ice content retards the
33 thawing process by the uptake of latent heat (Noetzli et al., 2007). Complex interrelationships such as these let permafrost
34 in superficial sediments respond merely slowly to climate forcing, i.e. within decades to centuries (cf. Haeberli et al.,
35 1997).

36 The Pellaud high mountain basin (Aosta Valley Autonomous Region, Northwestern Italy) is here presented since, being
37 affected by mass wasting processes (rock-falls and debris-flows), it allows to give a complete description of and apply the
38 methodology that has been developed (1) to analyse the stability of high mountain rock walls, from which rock-blocks
39 can be released, (2) to evaluate the stability of the rock-debris that due to the above collapses can deposit on the slope and
40 (3) to run numerical analyses to investigate the possible dynamic evolution that this loose material can have in terms of
41 debris-flow.

1 The first two parts of this methodology were elaborated in the activities B1-C1 of the RiskNat project. In particular, the
2 first of them is intended to identify the potentially unstable zones, on the basis of the geostructural and morphological
3 characteristics of the rock slopes, and to evaluate the effects of a possible permafrost degradation on the stability of the
4 cliff sectors. As a consequence, aim of this part of the work is in particular to address the following issues:

- 5 1. the geostructural conditions of the slopes;
- 6 2. the slope stability conditions as a function of the variation of the strength properties of the discontinuities due to
7 permafrost changes.

8 The importance of these two issues is relevant in high mountain basins because:

- 9 • the existing discontinuities tend to be open and to be affected by thaw-freezing cycles, thus exposing potentially
10 unstable blocks;
- 11 • the assessment of stability is linked not only to the orientation of the geo-structural planes and of the slope, but also to
12 the hydraulic and mechanical properties of the rock mass;
- 13 • the thaw-freezing cycles induce changes in the strength of the planes and in hydraulic conditions;
- 14 • the permafrost degradation can lead to a deepening of the active layer and to an increase of the depth concerned by
15 thaw-freezing cycles;
- 16 • the orientation of the planes of discontinuity is very often difficult and dangerous to assess because of environmental
17 conditions;
- 18 • the dimensions of the rock walls to examine are often wide;
- 19 • the basin geometry is a fundamental basis for all zoning issues (stability, danger etc. ..).

20 Once the potentially unstable zones have been identified for the Pellaud basin, the second part of the methodology, and of
21 the paper as well, is devoted to the stability analysis of the rock-debris that, due to the collapse of rock-blocks from cliff
22 walls, are deposited along the slope below. The debris are characterized by recurrent instability of the toe that evolves to
23 debris flow. It then becomes particularly important to understand how the thaw-freezing cycles can affect the rock-debris
24 deposits by analysing the influence of the ice content and of the debris friction angles. The unstable volumes are also
25 analysed.

26 Finally, the numerical simulations of the possible evolution of these deposits as debris-flow is undertaken.

27 The reduction of losses inferred by debris flows can be in fact pursued by prediction of their velocities and runout distances.
28 Indeed, runout prediction provides a mean of defining the susceptible areas, estimating the debris flows intensity (that is
29 an input of risk studies), and working out the information for the individuation and design of appropriate protective
30 measures. At the same time, reliable predictions of runout can help avoiding exceedingly conservative decisions regarding
31 the urban development of hazardous areas (Cascini et al., 2005).

32 At present, most practical runout predictions are empirical, making use of correlations among historical data (e.g.
33 Corominas, 1996; Zimmermann et al., 1997; Rickenmann, 1999). Though all of these methods are easy to use, they should
34 only be applied to conditions similar to those on which their development is based (Rickenmann, 2005).

35 A different and promising approach is that based on the continuum numerical modeling, whose models allow
36 determination of the flow parameters and deformation of the mass along the entire path, including deposition (e.g. O'Brien
37 et al., 1993; Iverson and Denlinger, 2001; McDougall and Hungr, 2005).

38 The numerical codes based on this last approach are at present largely used, even if 1) setting of rheological parameter
39 values for prediction purposes is troublesome, as a lack in information may prevent from obtaining them by resorting to
40 back analyses, and 2) results can be a function of the assumed rheology (Pirulli and Sorbino, 2008).

1 The continuum mechanics code RASH3D (Pirulli, 2005; Pirulli et al., 2007) has been here used to simulate the propagation
2 of the Pellaud potential debris flows. The results obtained with two different rheologies: the Voellmy and the Frictional,
3 and with different combinations of rheological values are compared and discussed.

4 5 **2. DESCRIPTION OF THE PELLAUD STUDY SITE**

6 The Pellaud catchment basin is located on the orographical left side of the upper Rhêmes Valley, a secondary valley of
7 Aosta Valley Region (Northwestern Italy) in the municipal district of Rhêmes Notre Dame. The catchment basin is shaped
8 like an amphitheatre on which the Becca dei Fos (3459 m asl), Grand Rousse Sud (3555 m asl) and Grand Rousse Nord
9 (3607 m asl) peaks overlook (Figs.1 and 2).

10
11 **Fig. 1** Small sketch with location of the Aosta Valley Region and detailed layout plan of the Pellaud basin.

12
13 The amphitheatre walls are made of metamorphic rock (gneiss and mica schist) and are about 500 m high, from 3550 m
14 asl to 3000 m asl; below there are steep slopes (always more than 30°) with some cliffs that end at 2200 m asl in the
15 alluvial fan where the Pellaud torrent runs up to the confluence (1810 m asl) with the main torrent of Rhêmes Valley, the
16 Dora di Rhêmes river. In the upper part of the basin there is a glacier (Pellaud Glacier) which has almost totally disappeared
17 leaving some loose material on the slopes (Curtaz et al., 2011) (Figs.1 and 2).

18
19 **Fig. 2** Description of the study area. Area 1: rock debris on the orographical left side of the Pellaud Torrent; Area 2: rock debris on the
20 orographical right side of the Pellaud Torrent

21
22 Rock material is periodically released from the above mentioned rock cliffs and accumulates on the steep slopes below,
23 until strong precipitations take it in charge and transport it to the valley floor, causing debris flows and mass wasting
24 events. In autumn 2005, some rock-falls originated from the eastern side of the Becca di Fos and, after being deposited on
25 the steep slopes below, were carried in the form of debris-flow to the lower part of the basin.

26 The helicopter surveys organized after the 2005 event evidenced the presence of some ice in the fractured rock mass and
27 in the scar of the rockfalls; this fact led to add value to the hypothesis that permafrost degradation and instability
28 phenomena could be correlated.

29 Other events produced during the next years (e.g. 2006-2007) and they continue to this day. The increase in the frequency
30 and in the magnitude of the debris flows also lead to stop the construction of the torrent protection measures that started
31 after the 1996 flood.

32 The site is still active and periodically strong precipitations repropose the same problem: surface runoff carries the rock
33 material deposited on the steep slope and transports it in the Pellaud Torrent producing debris flow events. The magnitude
34 of these events has been assessed variable in each event in the range 5000-15000 m³.

35 Based on the interpretation of the orthophotos taken during the 2011 flight over the Aosta Valley glaciers, the presence of
36 rock material deposited on the Pellaud upper slope was evidenced in two main areas:

- 37 - Area 1 (Fig. 2). On the orographical left side of the Pellaud Torrent, where glacial drift (i.e. the loose and unsorted rock
38 debris distributed by glacial melt waters) is originated by the Pellaud glacier;
39 - Area 2 (Fig. 2). On the orographical right side of the Pellaud torrent, immediately below the rock walls of the basin,
40 where rock material released from the cliff is deposited on steep slopes.

3. PHOTOGRAMMETRIC SURVEY

The photogrammetric survey of the area was carried out from a helicopter using a Nikon D3x camera (format 36x24mm, resolution 6048x4032) with a 35 mm lens; two strips were collected with very high forward overlap (more than 80%); the GSD (Ground Sampling Density) is about 7 cm. Block orientation has been performed by automatically finding tie points with a Structure from Motion algorithm implemented in EyeDea (Barazzetti et al, 2011); in each image, an average of about 500 tie points were measured; each point was imaged on average in 8 photos: in such a way, the inner block structure is very strong and a fair amount of reliable seed points is provided for the DSM (Digital Surface Model) generation.

Block georeferencing was performed by measuring about 30 ground control points from two theodolite stations in the valley. The estimated average accuracy for the tie points is about 2 cm in North and Elevation and about 6 cm in East direction. A dense point cloud of about 2106 points with an average spacing of 15 cm has been produced using Dense Matcher, a software using image correlation techniques developed at Department of Civil Engineer of University of Parma (DICATeA). In Fig. 3 the resulting 3D representation of the slope is represented.

Fig. 3 DSM 3D representation of the slope.

4. GEOSTRUCTURAL SURVEY

In order to carry out a stability analysis, it was necessary to survey the number and respective orientations of the discontinuity families in the examined rock mass. For this purpose a geostructural survey of the discontinuities was conducted using the ROCKSCAN program (Voyat et al., 2006; Ferrero et al., 2009, Ferrero et al., 2011), which allows to determine the orientation and position of conveniently chosen surface discontinuities automatically identified on the basis of the results of the photogrammetrical survey of the walls. The program, through opportune geometrical segmentation processes of the DSM, has made it possible to determine the equation of the plane that best approximates the geometry of the selected zone. The discontinuity planes were then identified on the photographs and, thanks to the coupling of these with the DSM of the examined wall, their position in space, and their immersion and dip values were defined.

Altogether 500 planes were identified, and the orientation (dip-dip direction), position and spacing were identified for each of these. The surveyed data were treated statistically using the DIPS program (Rocscience) in order to identify the discontinuity systems, their mean orientation and the characteristic spacing values. Three main discontinuity systems were identified: P1, P2, P3 (Fig. 4). It was then possible to analyze their kinematics and verify their stability.

Fig. 4 Stereographic projection and orientation angles of discontinuity systems.

5. ROCK-WALLS STABILITY ANALYSIS AND THEMATIC MAPS

The failure conditions of a rock wall are defined, generally, through kinematics analyses that allow the removability condition of the rock blocks to be defined and the following application of specific Limit Equilibrium Methods (LEMs) to identify stability conditions of finite and removable blocks.

Kinematic analyses apply a purely geometrical approach based on comparison between the discontinuity systems orientation and the slope orientation to define the failure modes that can be occurred in the rock mass. These analyses are based on the stereographic projection techniques of discontinuity and slope planes. Among the methods that apply these techniques the Markland's test (Markland, 1972; Hoek and Bray, 1981; Harrison and Husdon, 1997, Yoon et al., 2002) has been used in this study. It allows the identifications of four failure modes: planar sliding along a single plane or multiple planes, wedge sliding, block toppling and flexural toppling.

1 Once the possible cases of movement (possible kinematisms) have been identified for each combination of planes-slope,
2 it is possible to analyze the stability conditions, considering the forces that could cause the block moving and applying
3 LEMs. These methods consider rigid conditions of movements of the block along the discontinuities and they are based
4 on the balance of the forces acting on the block, defining a Factor of Safety FS defined as ratio between the stabilizing
5 and unstabilizing forces. The result of these analyses is expressed through a safety factor that quantifies the propensity to
6 mobilize of the possible cases of kinematics.

7 For each type of possible kinematism identified by Markland's test several analytical formulas can be applied (Hoek e
8 Bray, 1981; Hudson and Harrison, 1997) to determine the FS relating to the geometrical and discontinuity strength
9 conditions and to the considered acting forces (weight, water under-pressure, reinforced elements, ect).

10 5.1 Parametric analysis

11 Due to the extension of the studied area (2 300 000 m²) and the extremely variability of the local orientation of the slope,
12 the kinematic analysis and the following stability analyses were carried out dividing the whole area in a regular square
13 mesh, having a grid of 5mx5m.

14 The Markland's test has been applied comparing the orientation of the discontinuity systems identified by geosstructural
15 survey (Figure 4) and the local attitude of the slope defined as the mean orientation of each cell. It allowed to verify in
16 each cell the type of slope failure (kinematisms) connected to each of the three discontinuity planes (planar sliding), to
17 their lines of intersection (wedge sliding) and to the other combination of planes (flexural and block toppling). A thematic
18 map of the examined area (Figure 5.a) was then drawn up to represent the crossing result obtained; in some cells no case
19 of potential kinematism were defined whereas in other cells one or more type of failures were identified. In this way it has
20 been possible attribute to each cell a detachment propensity index, proportional to the number of different kinematisms
21 identified (see different colures of the cells in figure 5.a). The test pointed out that 39.2% of the examined cells can be
22 considered potentially unstable.

23 The stability analyses were carried out applying for each failure mode, varying the strength characteristics of the
24 discontinuities (friction angle and cohesion) and the hydraulic underpressure conditions, in order to simulate the freeze-
25 melting effect.

26
27 **Fig. 5** Thematic maps of kinematism and instability zones: a) detachment propensity index, proportional to the number of different
28 kinematisms identified in each cell (variable between 0-absence of failure possibility, to 6, co-presence of 6 different failure modes);
29 b) Factor of safety obtained in each cell from the stability analyses carried out considering the different failure mode (results obtained
30 with $\phi=35^\circ$ and zero cohesion).

31
32
33 The first parametric analysis carried out consisted in evaluating the influence of the decrease in discontinuities friction
34 angle value (40, 35 and 30°) on the safety factor value. As already mentioned, the safety factors were calculated with
35 formulas derived from the analysis of the limit equilibrium. From these analyses it emerges that the types of kinematism
36 in the examined basin with the highest percentages of probability of occurrence are flexural toppling with sliding along
37 P1, flexural toppling with sliding along P2 and tri-dimensional sliding along the Intersection line L 1-3 intersection line
38 (Fig. 6). Furthermore, the values of the safety factors decrease with the friction angle of the discontinuity, both in the case
39 of planar sliding and tri-dimensional sliding. However, it is possible to note that the percentage of actually unstable cells
40 does not vary with a variation of the friction angle of the discontinuity. This means that when the safety factor is below 1,
41 it remains so, even with a variation of the friction angle of the discontinuity. On the other hand, where the safety factor is
42 above 1, it remains so, although the value varies. This is not the case when flexural toppling is considered, as there are

1 more noticeable variations in the safety factor, and therefore in the percentage of unstable area, for variations of the friction
2 angle of the discontinuity.

3 Again in this case, thematic maps were drawn up in which the unstable cells ($FS < 1$) were colored red, the stable ones, but
4 which come close to the limit equilibrium condition ($1 < FS < 1.5$) were colored yellow, the stable cells ($FS > 1.5$) were
5 colored green and the cells in which no kinematism was previously pointed out were colored blue (Fig. 5.b). The maps in
6 Figure 5.b report the results obtained considering a friction angle of 30° . In this case is it possible to note that only about
7 the 26,5% of the basin area results instable.

8
9 **Fig. 6** Unstable area vs. apparent cohesion obtained for sliding along plane P1 by varying the value of discontinuity friction angle.

10
11 The second parametric analysis evaluated the influence of rock bridges (and therefore an apparent cohesion of
12 discontinuities) on the safety factor values for planar sliding phenomena and therefore the influence of the discontinuity
13 persistence.

14 Persistence represents the ratio between the discontinuous areas and the total reference area. Therefore, a persistence of
15 100% corresponds to an infinitely extended discontinuity condition, while a persistence of 0% corresponds to an intact
16 rock condition. In order to analyze the stabilizing effect of rock bridges, the discontinuity persistence was then gradually
17 decreasing in order to identify the value corresponding to the total stability. The stability analyses were carried out by
18 imposing to the discontinuity an apparent cohesion proportionally increasing to the considered rock bridge length.
19 Considering a reference value of cohesion for the intact rock of about 40 MPa, the discontinuity apparent cohesion value
20 was then derived multiply this value for a percentage equal to the relative rock bridge length. Because the observed joint
21 persistence is very high (98,9%, 98,4% and 97,4%), very short rock bridge were considered (1,1%, 1,6% and 2,6%).
22 Consequently, the apparent cohesion values imposed to the discontinuities are very low (0.40 MPa, 0.60 MPa, and 1.0
23 MPa, respectively).

24
25 The results (Fig. 7). show how the presence of even very small rock bridges can drastically reduce the percentage of the
26 unstable area; for example, the unstable area of 1.26% for planar sliding along plane P1 (Fig. 7) with a friction angle of
27 the discontinuity of 35° in infinitely extended conditions, is reduced to 0.13% (decrease of 89.05% compared to the
28 previous situation) for a persistence of 98.9%. The same was verified for planar sliding along the P2 plane, with a friction
29 angle of the discontinuity of 35° , as there is an unstable area percentage of 0.94% in infinitely extended discontinuity
30 conditions, while for a persistence of 98.9%, the unstable area is reduced to 0.04%, with a decrease of 95.7%. For planar
31 sliding along P3, instead, there are no cases of potential kinematics, therefore the unstable area results to be nil. The
32 analysis has also pointed out that, with a persistence of 97.4% (apparent cohesion of 1MPa), total stability conditions are
33 reached for all the considered cases of kinematism.

34
35 **Fig. 7** Unstable area vs. discontinuity friction angle obtained for sliding along plane P1 by varying the value of apparent cohesion.

36
37 The third parametric analysis investigated the role of water presence, and therefore different hydraulic underpressure
38 hypotheses. The following configurations were considered in particular:

- 39 • the presence of hydraulic underpressure along the sliding plane (U);
- 40 • the presence of hydraulic underpressure along the sliding plane + tension crack (U+V).

41 The analysis was only performed for planar sliding and the presence of rock bridges was not considered.

1 For each examined kinematism, the percentage of unstable area does not depend on the two hydraulic configurations or in
2 consideration of the friction angle of the discontinuity. In fact, all the cells where a potential kinematism was identified
3 (both for planar sliding along plane P1 and for planar sliding along plane P2) resulted to be unstable, while no example of
4 kinematism was found for planar sliding along plane P3. What does vary between the two configurations is obviously the
5 safety factor value, FS, which, however, always remains below 1 and sometimes even takes on negative values. As in the
6 other two cases, thematic maps were drawn up to represent the results.

7 Crossing the results of the different stability analyses, it results that 52.3% of the cells in which potential kinematisms
8 were identified, are unstable. Overall, the unstable area is equal to 20.5% of the total area of the examined basin, so of
9 about .

10
11
12 In conclusion, the substantial importance of cohesion on the discontinuities, from the mechanical point of view, has been
13 pointed out. This cohesion is due to the strength of the rock bridges: in many cases, a very low percentage of rock bridges
14 (less than 2%) is sufficient to guarantee stability of the blocks. This result confirms the probable progressive mechanism
15 of block detachment, due to the rupture of rock bridges, because of cyclic loading phenomena caused by alternations of
16 freezing and melting of the water inside the fractures. The presence of hydraulic underpressure is in fact due to the
17 possibility of a greater water circulation during the melting phases, and the variations in temperature influence the
18 evolution of instability, at least in an indirect manner.

19 20 **6. STABILITY ANALYSES OF THE ROCK-DEBRIS DEPOSIT**

21 A series of 2-dimensional stability analyses, performed using Slide code (Rocscience) based on Limit Equilibrium Method
22 (LEM), was carried out to study the stability conditions of the rock-debris deposit (Area 1 in Fig. 2) under different climate
23 conditions. The analyses were carried out along a vertical section obtained by the DSM (Fig. 3) and considering a
24 simplified profile in which the bedrock position has been reconstructed by examining the areas of the slope not covered
25 by ice.

26 The principal aim of the LEM analyses is to understand how the thaw-freezing cycles can affect the rock-debris deposits
27 when they are subjected to permafrost. Three different scenarios have been so considered:

- 28 • absence of permafrost (Fig. 8a) with a variable water table height H_w to simulate all the conditions of saturation:
29 from the absence of water to the complete saturation of the debris deposit;
- 30 • freezing phase (Fig. 8b): it is typical of the autumnal season when the environmental temperature decreasing
31 leads a lowering temperature of the deposit from the outer to the inner layers and to the consequent formation of
32 frozen layer confining the saturated debris material;
- 33 • thawing Phase (Fig. 8c): it is typical of spring season characterized by an increase of the environmental
34 temperature that corresponds to an increasing temperature of the deposit starting from the outer layers toward the
35 inner ones. This induces a decreasing of the material cohesion and the water formation due to ice melting in the
36 shallower layers.

37 To evaluate how the alternation of frozen-no frozen layers, with changing temperatures, affects the deposit stability
38 conditions, this latter was subdivided in layers having an average thickness of 2m. Each layer was characterised by a
39 different strength parameter, following the Mohr Coulomb criterion. The observation of the natural dip of the slope where
40 the debris material is located has allowed the authors to define a possible range of variation of the friction angle of the
41 debris material: it was considered ranging from 36° to 52° depending on its level of compaction and its grain size

1 distribution. The frozen material was characterised by a friction angle equal to that of the debris material and a cohesion
2 due to the presence of ice in the intergranular spaces. The value of cohesion was determined from the results of uniaxial
3 compressive tests (UCS) carried out on cylindrical frozen specimens varying their temperature conditions from -1.5° to -
4 28°C (Ferrero et al, 2014; Curtaz et al, 2012). As the aim of the LEM analysis is to study the thaw-freezing phases
5 characterised by a temperature close to zero, it was attributed to this material a UCS of 3.800 MPa corresponding to a
6 temperature of -1,5°C and the cohesion values reported in Table 1.

7 In Fig. 8 a not-scaled sketch of the analysed sections with the geometrical parameters is reported.
8

9 **Table 1** Mohr-Coulomb strength parameters used in the LEM analyses
10

11 **Fig. 8** Not scaled sketch of the analysed section reporting the geometrical setting: a) No-permafrost analyses; b) Freezing
12 phase analyses; c) Thawing phase analyses; d) evaluation of the unstable slope degree D_{UN}
13

14 All the analyses were carried out by varying the strength characteristics of the materials and the water table position H_w
15 in no-permafrost analyses (analyses with no ice), or the thickness T_F and position of frozen layer in the thaw-freezing
16 analyses.

17 The instability conditions were evaluated defining an unstable degree of the deposit defined as the percentage of unstable
18 area D_{UN} , computed as:

$$D_{UN} = \frac{A_{UN}}{A_{DEP}} 100$$

19
20
21 where A_{UN} is the unstable area, computed as the area comprises between the critical sliding surface (to which corresponds
22 the deeper sliding surface having a FS lower than 1) and the slope profile and A_{DEP} is the area of the whole debris deposit.
23 The first set of analyses was performed considering no-frozen saturated debris material and varying the water table height
24 H_w from zero (completely dry material) and 24 m (completely saturated material). The Fig. 9 shows the relation between
25 the water height and the unstable degree for the two limit strength values of the no-frozen material.

26 If the material is characterised by a low strength value (ϕ equal to 36°), the stability conditions are strongly affected by
27 the presence of water. In this case, the unstable degree is equal to about 7% of the whole debris area with a water height
28 of 2 m, but its value reach 70% with a total saturation of the debris deposit. On the contrary, when the strength value
29 increases (ϕ equal to 52°) the unstable areas are localised to the deposit toe and the mobilised area remain lower than 8%.
30

31 **Fig. 9** Water height (H_w) vs. unstable Degree (D_{UN}) obtained from no-frozen analyses considering the two limits values
32 of debris strength parameters.
33

34 The analyses carried out to evaluate the effects of thaw-freezing cycles were performed by varying thickness and position
35 of the frozen layers, as illustrated in Fig. 10. To simulate the freezing phase, the deposit was considered as composed by
36 two different layers: an upper frozen layer having a variable thickness T_F and a lower saturated no-frozen layer. In this
37 case, the freezing process was simulated lowering the position of ice-water interface.

38 On the contrary, the thawing phase was simulated with a raising ice-water interface and so, with a lower frozen layer,
39 having a variable thickness T_F , and an upper saturated debris layer.
40

1 **Fig. 10** Thickness of frozen material (T_F) vs. unstable Degree (D_{UN}) obtained from thaw-freezing analyses considering
2 the two limits values of debris strength parameters.

3
4 Also in this case, if the material has a high value of strength angle, the stability condition shows limited changes with the
5 thickness of frozen layer, neither during the thaw phase nor in freezing one. If the material has lower strength values, the
6 stability conditions are strongly affected not only by the thickness of the frozen layer but also by the acting environmental
7 process. Fig. 10 shows that for thickness higher than 18 m the deposit can be consider stable ($Dun < 2\%$). If the frozen
8 layers are smaller, the unstable degree can reach values equal to 55-65%, both in thawing and freezing processes. In this
9 case, the worst stability condition is evident during the thawing phases, because at the same value of frozen thickness
10 corresponds a higher value of the unstable volume.

11 This part of the work showed the strong influence of climate and water phase change in particular on the debris instability.
12 The triggering of the debris is due to combination of the ice presence and of the intrinsic strength features of the debris
13 strongly influenced by the environmental conditions. The high percentage of unstable debris in the case of low friction
14 angle and low ice presence is not realistic since it would deal to very high unstable volume. Based on the volume of
15 material handled during the construction of some mitigation structures along the Pellaud Torrent in 1998, the volume
16 involved in a single past debris flow event was estimate to range between 5000 and 15000 m³. Since debris volume varies
17 between 5000 and 15000 m³ and the surface extension of the debris has been estimated in about 27000m² the debris friction
18 angle is possibly closer to 52° then to 36° and the ice is possibly not melting completely during summer. On this basis, it
19 is realistic to estimate unstable volume between 1% and 3% of the global debris deposit developing from the deposit face
20 in spring or in autumn during the water phase change.

21 22 **7. RUN-OUT ANALYSES**

23 Run-out analyses are here intended to study the consequences of the possible evolution in terms of debris-flow of the rock-
24 debris that exists deposited on the Pellaud slope.

25 The RASH3D code, which is based on a continuum mechanics approach and whose governing balance equations are based
26 on the depth-averaged (St. Venant) shallow-water equations, is used to this aim. Full details of its formulation and
27 implementation were presented in Pirulli (2005). The model treats the landslide mass as an “equivalent fluid” (Hungr,
28 1995), a hypothetical material that is governed by simple rheological laws. The internal rheology is assumed to be
29 frictional, while the basal rheology, which controls the basal shear stress, must be constrained by calibration using
30 prototype events. A number of basal rheologies are implemented, including the Frictional and the Voellmy that are here
31 applied to study the potential instabilities in the Pellaud basin.

32 Three steps are necessary to run numerical analyses with RASH3D: 1) uploading the topography of the study area as a
33 DEM (Digital Elevation Model), 2) determining the event initial volume, and 3) calibrating the rheological parameters.

34 The main uncertainties for modelling the potential events concerned:

35 - the estimation of the initial volume. In consideration of the potentially unstable areas described in Section 2 and
36 represented in Fig. 2, this problem was faced by defining two different scenarios in terms of triggering areas: Scenario
37 A: Area 1; Scenario B: Area 2, and for each scenario, according to the volume estimations described in the previous
38 section, two different volumes were released: 5000m³ (Scenarios A1 and B1) and 15000m³ (Scenarios A2 and B2),
39 respectively.

40 - the selection of the rheological law and the setting of its parameter values. Since detailed data of past events were not
41 available, this problem was faced by running analyses with two different rheologies (Frictional vs. Voellmy) and

1 defining rheological parameter values by data obtained from scientific literature for systematic back-analysis of similar
 2 events (e.g. Quan Luna et al., 2010). A kind of parametric analysis procedure was then used to evidence the importance
 3 of rheological setting on numerical simulation results.

4 The Frictional rheology is based on a constant friction angle δ , which implies a constant ratio of the shear stress to the
 5 normal stress. The shear resistance stress is independent of the velocity:

$$6 \quad \tau = (\rho g_z h \tan \delta) \text{sgn}(\bar{v}) \quad (1)$$

7 where ρ is the material bulk density, g_z is the acceleration due to gravity in the $-z$ direction that is normal to the
 8 topography, h is the flow depth and \bar{v} is the depth-averaged flow velocity.

9 The Voellmy rheology (Voellmy, 1955), which consists of a turbulent term, ξ , that accounts for velocity-dependent
 10 energy losses, and a Coulomb or basal friction term to describe the stopping mechanism. The resulting basal shear
 11 stress is given by the following equation:

$$12 \quad \tau = \left(\rho g_z h \mu + \frac{\rho g \bar{v}^2}{\xi} \right) \text{sgn}(\bar{v}) \quad (2)$$

13 where ξ is the turbulence coefficient and μ is the friction coefficient, with $\mu = \tan \delta$.

14 7.1 Results of the numerical analyses

15 A set of numerical analyses was carried out for Scenario A1 to have a comparison between results that can be obtained
 16 using the two different rheologies (i.e. Frictional and Voellmy). The range of values for each rheology was defined on the
 17 basis of both the Authors' personal experience on the analysis of this type of phenomena (e.g. Pirulli, 2010; Pirulli and
 18 Marco, 2010; Pirulli and Sorbino, 2008) and the existing literature treating for events with characteristics similar to the
 19 here investigated case (e.g. Hungr and Evans, 1996).

20 The two combinations of rheological values that were finally selected and here presented for each rheology are intended
 21 to evidence the important role of rheology calibration on numerical analysis results. In fact, as it will be evidenced in the
 22 following, these combinations of values represent the lower and upper boundary of the rheological values that respectively
 23 determine the minimum and maximum extension of the area involved by the potential movement. It is obvious that a
 24 further increment of the frictional parameter could prevent the mass from triggering and a further increment of the
 25 turbulence coefficient could make the mass running further but in the first case the phenomenon would lose meaning in
 26 terms of propagation while in the second one the mass would continue running along the Dora di Rhemes course.

27 As a result, Fig. 11 presents the maximum run-out depths of the flowing mass during the whole propagation process (from
 28 triggering to deposition) obtained with a Frictional rheology setting $\delta = 15^\circ$ (Fig. 11a) and $\delta = 25^\circ$ (Fig. 11b), respectively,
 29 and with a Voellmy rheology for the combinations of parameters $\mu = 0.1 - \xi = 500\text{m/s}^2$ (Fig. 11c) and $\mu = 0.05 - \xi =$
 30 1000m/s^2 (Fig. 11d), respectively.

31
 32 **Fig.11** Scenario A1. Results of the numerical analyses carried out with the RASH^{3D} code. Frictional rheology: a) $\phi = 15^\circ$, b) $\phi = 25^\circ$.
 33 Voellmy rheology: c) $\mu=0.1 - \xi = 500\text{m/s}^2$, d) $\mu=0.05 - \xi = 1000\text{m/s}^2$.

34
 35 It can be observed that, according to Pirulli (2010), the use of a frictional rheology is not recommended for the run-out
 36 analysis of a debris-flow; in fact, contrary to what was observed for real past event, the moving mass, instead of running
 37 along the Pellaud torrent track, follows a linear trajectory. This is due to the limit of the frictional rheology of
 38 overestimating velocities. On the contrary, numerical results obtained with both the Voellmy combinations of parameters

1 evidence the capability of the model in reproducing the run-out path that was followed by past events. A change of its
2 rheological values can only cause a decrease or an increase in the runout distance reached by the moving mass, in case of
3 Fig. 11c the mass deposits on the slope while, in case of Fig. 11d the flowing mass reaches the valley bottom and at the
4 intersection with the Dora di Rhemes river canalizes along the main river track. Finally, a detailed analysis of Fig. 11c and
5 of the underneath orthophoto evidences that the area where the simulated mass deposits is really covered by rock blocks
6 deposited by past events (Fig. 12). Similarly, a detailed analysis of Fig. 11d evidences that the good quality of the adopted
7 DEM (courtesy of the Aosta Valley Region) has allowed the simulated mass to follow with high precision the track of the
8 torrent before and of the river after (Pirulli and Marco, 2010).

9
10 **Fig. 12** Details of the Pellaud channel. Arrows indicate the presence of rock blocks deposited during past events. The contour interval
11 is 20 m.

12
13 Moving to the analysis of Scenario B1, the use of the frictional rheology has not been pursued according to the above
14 observations. Results obtained for the Voellmy rheology are represented in Fig. 13.

15
16 **Fig. 13** Scenario B1. Results of the numerical analyses carried out with the RASH^{3D} code. Voellmy rheology: a) $\mu=0.1$ - $\xi = 500\text{m/s}^2$,
17 b) $\mu=0.05$ - $\xi = 1000\text{m/s}^2$.

18
19 The release of the debris deposited on the slope due to the collapse of rock-blocks from the basin rock-walls evidenced a
20 behaviour similar to that evidenced in case of Scenario A1. But, in case of Scenario B1, due to the position of the triggering
21 area that is closed to the watershed divide, a part of the volume, instead of being channelized along the Pellaud torrent,
22 gives rise to a second propagation branch in portions of the slope that, from detailed analysis of the orthophoto result
23 interested by the presence of a hydrographic net where the presence of transported and deposited loose material can be
24 evidenced. However the small quantity of material in this area is also evidenced by the numerical simulations through the
25 very small maximum depths that the moving mass has here had (Fig. 13b).

26
27 Finally, the most destructive scenarios, A2 and B2, each involving 15000m^3 of released material were simulated with the
28 Voellmy rheology, Obtained results are grouped in Fig. 14.

29
30 **Fig. 14** Results of the numerical analyses carried out with the RASH^{3D} code. Scenario A2 - Voellmy rheology: a) $\mu=0.1$ - $\xi = 500\text{m/s}^2$,
31 b) $\mu=0.05$ - $\xi = 1000\text{m/s}^2$. Scenario B2 - Voellmy rheology: c) $\mu=0.1$ - $\xi = 500\text{m/s}^2$, d) $\mu=0.05$ - $\xi = 1000\text{m/s}^2$.

32
33 As already mentioned, the two combinations of values here presented for the Voellmy rheology have been selected since
34 they can be assumed as the boundary values that for each analysed scenario allow to evidence the minimum and the
35 maximum extension of the area involved by the possible propagation of the unstable mass. The transition from one result
36 to the other can be considered as a function of the water content of the flowing mixture.

37 The analysis of these scenarios evidenced that, in both these cases, independently from the triggering area and from the
38 rheological parameter values, the simulated run-out area in the alluvial fan results approximately the same.

39 In terms of impact on the territory it can be observed that along the Dora di Rhemes river the mass remains channelized
40 while on the alluvial fan immediately below the Pellaud torrent the involved areas do not present high vulnerability, since
41 these are uninhabited areas. As to the Pellaud and Chaudanne hamlets, the simulation results evidence a partial

1 involvement of the hamlets in the run-out of the mass, in particular the Pellaud hamlet presents a more critical situation
2 due to the Pellaud channel bend immediately before the hamlet (Fig. 15).

3
4 **Fig. 15** Involvement of the Pellaud and Chaudanne hamlets in the run-out of the moving mass as obtained by numerical analyses.

5 6 **8. DISCUSSION AND CONCLUSIONS**

7 Alpine basins are often characterized by different kinds of instability phenomena that are chained one to the other: rock
8 fall, sliding and toppling of rock blocks on the upper part of the basin, rotational sliding of the glacial debris powered by
9 the rock blocks deposit that can finally evolve in debris flow with high mobility and destructive energy.

10 The paper was aimed to show a complete study able to analyze all the different parts of the basin with advanced survey
11 and computing methods. Temperature influence has also been taken into consideration since a certain seasonality of the
12 phenomena has been observed.

13 The paper has been divided in three parts: analysis of the rock walls, analysis of the rock debris deposits and analysis of
14 the debris flows. Some key issues have been identified for each part.

15 For the rock walls:

- 16 • the use of a photogrammetric survey from helicopter, as basis for the geostructural analysis done by means of
17 ROCKSCAN software, allows to get detailed data, avoiding direct contact with the rock face, often unstable.
18 The survey time is reduced and a wider area can be inspected;
- 19 • the availability of high resolution DEM model allows to extend the study to all the basin and to recognize which
20 type of kinematics can produce, where and which could be the influence of permafrost degradation inside the
21 rock mass;
- 22 • the results show the major role of the presence of rock bridges on stability and the susceptibility of these to
23 permafrost degradation due to freeze-melting cycles and water circulation and underpressure inside the fractures.

24 For the rock debris deposits:

- 25 • the debris deposit stability is conditioned by intrinsic debris features, such as the friction angle, and environmental
26 features such as the water/ice content and their temperature that determine the debris strength characteristics;
- 27 • the debris cannot be characterized by means of traditional geotechnical tests due to the large variability of the
28 blocks dimensions so only back analysis can be carried on to define the debris failure mechanism. Results showed
29 the major importance of the debris strength angle.

30 For the debris flows:

- 31 • the parametric analysis has shown how the rheology plays an important role in the simulation of the flow
32 dynamics. Of the two investigated rheologies, the Voellmy model produced the most consistent results in terms
33 of debris spread and distribution as well as velocity data. The main drawbacks of the frictional model are the
34 tendency to overestimate velocities and therefore to predict excessive spreading of the mass;
- 35 • the use of a high quality DEM allowed to simulate in an accurate way the mass propagation and highlighted the
36 importance of using suitably refined digital terrain data to evaluate the reliability of numerical results and the
37 associated calibrated rheological parameters;
- 38 • the selection of the rheological parameter value remains one of the major significant challenges. A calibration-
39 based approach is here considered as one of the most promising ways, given the difficulty in defining a relation
40 between static and dynamic parameters.

1 Concerning the Pellaud study area, the application of the above described advance survey and modeling techniques has
2 evidenced that, in this site environmental conditions, a volume of debris can become unstable and propagate up to the
3 valley bottom where some hamlets exist. In particular, in terms of impact on the territory it can be observed that along the
4 Dora di Rhemes river the mass remains channelized while on the alluvial fan immediately below the Pellaud torrent the
5 involved areas do not present high vulnerability, since these are uninhabited areas. As to the Pellaud and Chaudanne
6 hamlets, the simulation results evidence a partial involvement of the hamlets in the run-out of the mass, especially due to
7 the Pellaud channel bend immediately before the hamlet.

9 9. ACKNOWLEDGEMENTS

10 This work has been realized and funded in the framework of the project RiskNat (2007-2013 Operational program for
11 cross-border cooperation Italy - France, Alps - ALCOTRA), in particular in activities B1-C1 "Hazards deriving from high
12 mountain environment evolution" in collaboration with Fondazione Montagna Sicura.

14 10. REFERENCES

- 15 Barazzetti L, Forlani G, Remondino F, Roncella R, Scaioni M (2011) Experiences and achievements in automated image
16 sequence orientation for close-range photogrammetric projects. In: Proceedings SPIE 8085, Videometrics, Range Imaging,
17 and Applications XI, 80850F, Munich, Germany.
- 18 Cascini L, Bonnard C, Corominas J, Jibson R, Montero-Olarte J (2005) Landslide hazard and risk zoning for urban
19 planning and development (State of the Art Report). In: Proceedings of the International conference on landslide risk
20 management, Edited by: Hungr O, Fell R, Couture R, Eberhardt E, A.A. Balkema, Rotterdam, The Netherlands.
- 21 Censicro (2009) Censimento dei Crolli in Roccia in alta quota. Relazione tecnica finale Ing. Michèle CURTAZ. Internal
22 report.
- 23 Corominas J (1996) The angle of reack as a mobility index for small and large landslides. *Can. Geotech. J.* 33:260-271.
- 24 Curtaz M, Ferrero AM, Roncella R, Segalini A, Umili G (2014) Terrestrial Photogrammetry and Numerical Modelling
25 for the Stability Analysis of Rock Slopes in High Mountain Areas: Aiguilles Marbrées case. *Rock Mechanics and Rock*
26 *Engineering* 47(2): 605-620. DOI 10.1007/s00603-013-0446-z, ISSN 0723-2632.
- 28 Curtaz M, Ferrero AM, Forlani G, Migliazza M, Roncella R, Vagliasindi M (2011) Test of a procedure to assess the
29 stability of permafrost rock walls: the case of Pellaud basin, Rhêmes Valley (Aosta Valley, Italy). In: *Landslide Science*
30 *and Practice*, 4: 391-392, C. Margottini (Ed.). Proceedings of the Second World Landslide Forum, Rome, Italy.
- 31 Curtaz M, Ferrero AM, Migliazza M (2012) Study on the mechanical degradation of a frozen Alpine soil. In: Proceedings
32 of the 10th International Conference on Permafrost Resources and Risks of Permafrost Areas in a Changing World TICOP.
33 The Northern Publisher. Volume 1: 100-108.
- 34 Ferrero AM, Migliazza M, Roncella R, Segalini A (2011) Rock cliffs hazard analysis based on remote geosstructural
35 surveys: The Campione del Garda case study (Lake Garda, Northern Italy). *Geomorphology* 125(4): 457-471. ISSN 0169-
36 555X, DOI: 10.1016/j.geomorph.2010.10.009.
- 38 Ferrero AM, Forlani G, Roncella R, Voyat HI (2009) Advanced geo structural survey methods applied to rock mass
39 characterization. *Rock mechanics and Rock Engineering* 42(4):631-665.
- 40 Ferrero AM, Godio A, Migliazza M, Sambuelli L, Segalini A, Théodule A (2014) Geotechnical and Geophysical
41 Characterization of frozen granular material. In: *Landslides in Cold Regions in the Context of Climate Change*. Edited by:
42 Shan W, Guo Y, Wang F, Marui H, Strom A. Springer. 205-218 .
- 43 Gruber S, Hoelzle M, Haeberli W (2004) Permafrost thaw and destabilization of Alpine rock walls in the hot summer of
44 2003. *Geophys. Res. Lett.* 31: L13504.

- 1 Haeberli W, Wegmann M, Vonder Muhll D (1997) Slope stability problems related to glacier shrinkage and permafrost
2 degradation in the Alps. *Eclogae Geologicae Helvetiae* 90(3):407-414.
- 3 Harris C, Arenson LU, Christiansen HH, Etzelmüller B, Frauenfelder R, Gruber S, Haeberli W, Hauck C, Hölzle M,
4 Humlum O, Isaksen K, Kääb A, Kern-Lütschg MA, Lehning M, Matsuoka N, Murton JB, Nötzli J, Phillips M, Ross N,
5 Seppälä M, Springman SM, Vonder Mühll D (2009) Permafrost and climate in Europe: Monitoring and modelling thermal,
6 geomorphological and geotechnical responses. *Earth-Science Reviews* 92:117-171.
- 7 Hoek E, Bray JW (1981) *Rock Slope Engineering: Third Edition* CRC Press ISBN: 0-419-16010-8.
8
- 9 Hudson J, Harrison JP (1997) *Engineering Rock Mechanics. An Introduction to the Principles.* Elsevier Ltd.
10 ISBN: 978-0-08-043864-1.
11
- 12 Hungr O (1995) A model for the runout analysis of rapid flow slides, debris flows, and avalanches. *Canadian Geotechnical*
13 *Journal* 32 (4):610-623.
- 14 Hungr O, Evan SG (1997) Rock avalanche runout prediction using a dynamic model. *Landslides*, Senneset (ed), Balkema,
15 Rotterdam:233-238.
- 16 Iverson RM, Denlinger RP (2001) Flow of variably fluidized granular masses across three-dimensional terrain – 1:
17 Coulomb mixture theory. *J. Geophys. Res.* 106(B1):537-552.
- 18 Jomelli V, Pech P, Chochillon C, Brunstein D (2004) Geomorphic Variations of Debris Flows and Recent Climatic Change
19 in the French Alps. *Climatic Change* V64(1):77-102.
- 20 Jomelli V, Brunstein D, Grancher D, Pech P (2007) Is the response of hill slope debris flows to recent climate change
21 univocal? A case study in the Massif des Ecrins (French Alps). *Climatic Change* 85(1-2):119-137.
- 22 Markland, J.T. (1972). A useful technique for estimating the stability of rock slopes when the rigid wedge sliding type of
23 failure is expected. *Imp. Coll. Rock Mech. Res. Rep.* 19, 10.
- 24 McDougall S, Hungr O (2005) Dynamic modelling of entrainment in rapid landslides. *Can. Geotech. J.* 42(5):1437-1448.
- 25 Noetzli J, Gruber S, Kohl T, Salzmann N, Haeberli W (2007) Three-dimensional distribution and evolution of permafrost
26 temperatures in idealized high-mountain topography. *Journal of Geophysical Research* 112:F02S13.
- 27 O'Brien JS, Julien PY, Fullerton WT (1993) Two-dimensional water flood and mudflow simulation. *J. Hydrol. Eng.*
28 119(2):244-261.
- 29 Pirulli M (2005) Numerical modelling of landslide runout - A continuum mechanics approach. PhD Thesis in Geotechnical
30 Engineering, Politecnico di Torino, Italy.
- 31 Pirulli M, Bristeau MO, Mangeney A, Scavia C (2007) The effect of the earth pressure coefficients on the runout of
32 granular material. *Environmental Modelling & Software* 22(10):1437-1454.
- 33 Pirulli M, Sorbino G (2008) Assessing potential debris flow runout: a comparison of two simulation models. *Natural*
34 *Hazards and Earth System Sciences* 8:961-971.
- 35 Pirulli M, Marco F (2010) Description and numerical modelling of the October 2000 Nora debris flow, Northwestern
36 Italian Alps. *Canadian Geotechnical Journal* 47(2):135-146.
- 37 Pirulli M (2010) Morphology and substrate control on the dynamics of flowlike landslides. *Journal of Geotechnical and*
38 *Geo-environmental Engineering* 136(2):376-388.
- 39 Quan Luna B, van Westen CJ, Jetten V, Cepeda J, Stumpf A, Malet JP, Medina-Cetina Z, van Asch TWJ (2010) A
40 preliminary compilation of calibrated rheological parameters used in dynamic simulations of landslide run – out. In:

- 1 Mountain risks: bringing science to society - Proceedings of the Mountain Risks International Conference. Edited by:
2 Malet JP, Glade T, Casagli N. CERIG, Strasbourg, 255–260.
- 3 Ravanel L, Deline P (2011) Climate influence on rockfalls in high-Alpine steep rockwalls: The north side of the Aiguilles
4 de Chamonix (Mont Blanc massif) since the end of the ‘Little Ice Age’. *The Holocene* 21(2):357-365.
- 5 Rebetz M, Lugon R, Baeriswyl PA (1997) Climatic change and debris flows in high mountain regions: the case study of
6 the Ritigraben torrent (Swiss Alps). *Climatic Change* V36(3):371-389.
- 7 Rickenmann D (1999) Empirical relationships for debris flows. *Natl. Hazards* 19(1):47–77.
- 8 Rickenmann D (2005) Runout prediction methods. In: *Debris-flow Hazards and Related Phenomena*. Edited by: Jakob M,
9 Hungr O. Springer Praxis, Heidelberg, Germany, 305-324.
- 10 Rocscience code (<https://www.rocscience.com/products/1/Dips>)
- 11 Sattler K, Keiler M, Zischg A, Schrott L (2008) Relation between changes in debris-flow activity and degradation of alpine
12 permafrost – a case study from the Schnalstal, Southern Oetztal Alps. *Geophysical Research Abstracts* 10: EGU2008-A-
13 09855
- 14 Schoeneich P, Dall’Amico M, Deline P, Zischg A (2011) Hazards related to permafrost and to permafrost degradation.
15 PermaNET project, state-of-the-art report 6.2. On-line publication ISBN 978-2-903095-59-8.
- 16 Voellmy A (1955) Über die Zerstörungskraft von Lawinen. *Schweizerische Bauzeitung* 73:212-285.
- 17 Voyat IH, Roncella R, Forlani G, Ferrero AM (2006) Advanced techniques for geo structural surveys in modelling
18 fractured rock masses: application to two Alpine sites. *GoldenRocks 2006: 41st U.S. Rock Mechanics Symposium*,
19 Golden, Colorado.
- 20 Yoon W.S., Jeong, U.J., J.H Kim (2002). Kinematic analysis for sliding failure of multi-faced rock slopes. *Engineering*
21 *Geology* 67, pp. 51–61.
- 22 Zimmermann M, Mani P, Gamma P, Gsteiger P, Heiniger O, Hunziker G (1997) Murganggefahr und Klimaänderung -
23 ein GIS-basierter Ansatz. Schlussbericht NFP 31, vdf Hochschulverlag an der ETH, Zürich, 161 p.
- 24 Zischg A, Curtaz M, Galuppo A, Lang K, Mayr V, Riedl C, Schoeneich P (2011) Chapter 2: Permafrost and debris-flows.
25 In Schoeneich P. et al. (eds): Hazards related to permafrost and to permafrost degradation. PermaNET project, state-of-
26 the-art report 6.2. On-line publication ISBN 978-2-903095-59-8, p.29-66.

27

1

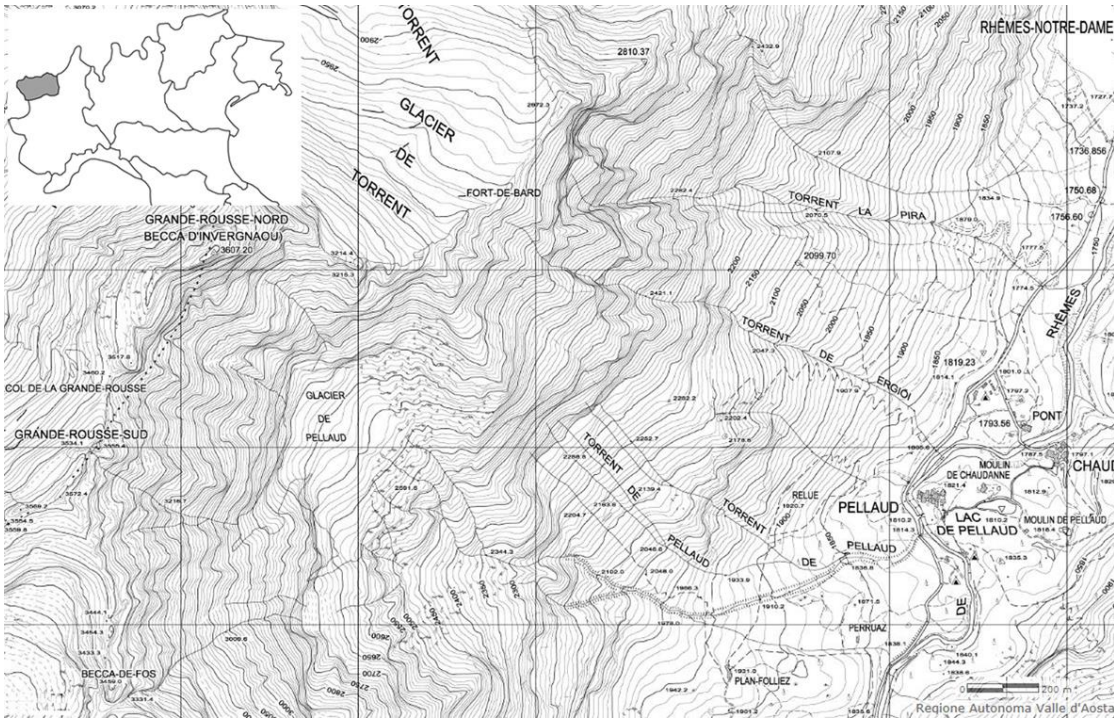
2

Table 1 Mohr-Coulomb strength parameters used in the LEM analyses

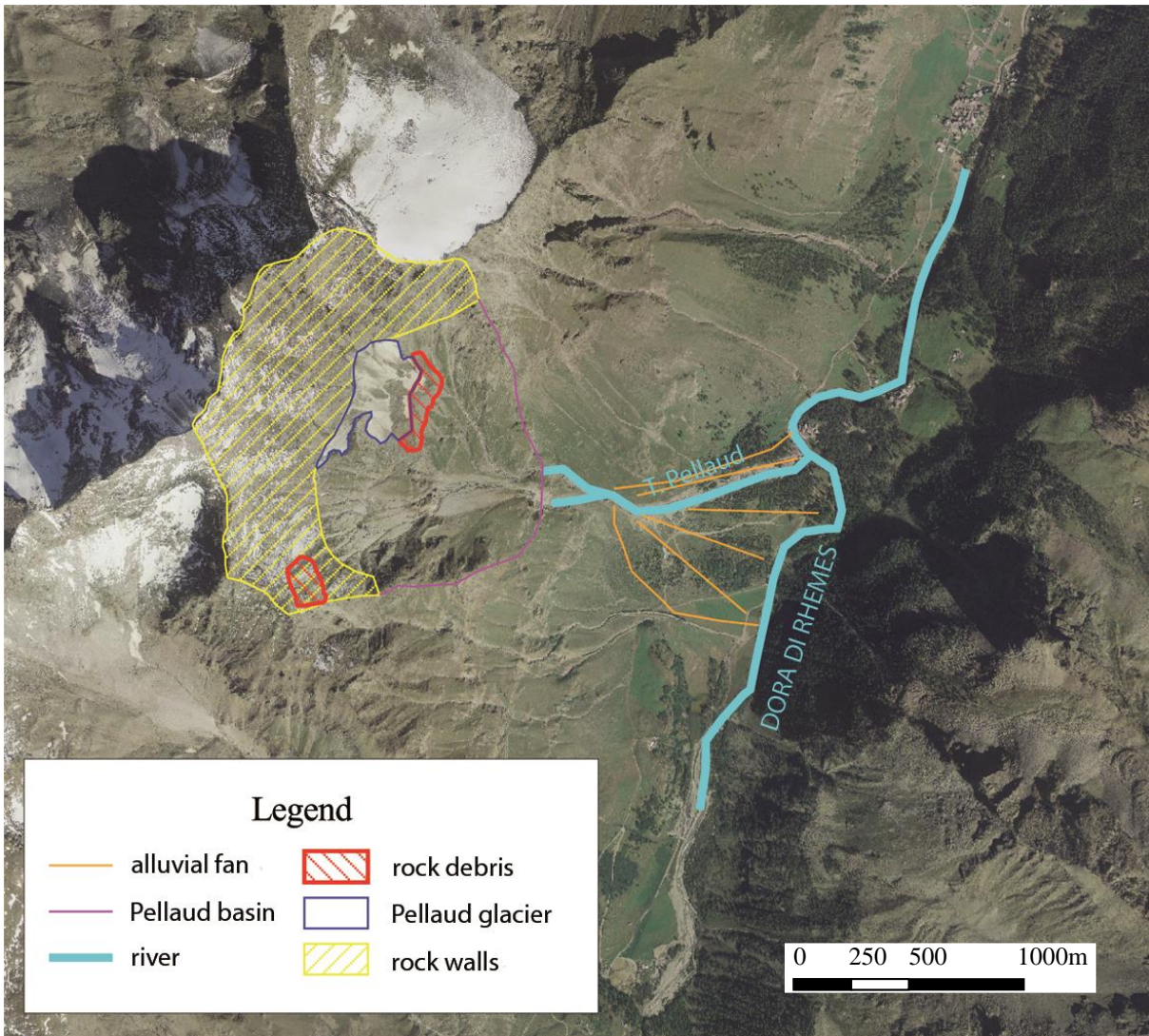
Rock - debris	Frozen material	
Friction angle ϕ [°]	Friction angle ϕ [°]	Cohesion c [kPa]
36	36	3870
52	52	2600

3

4

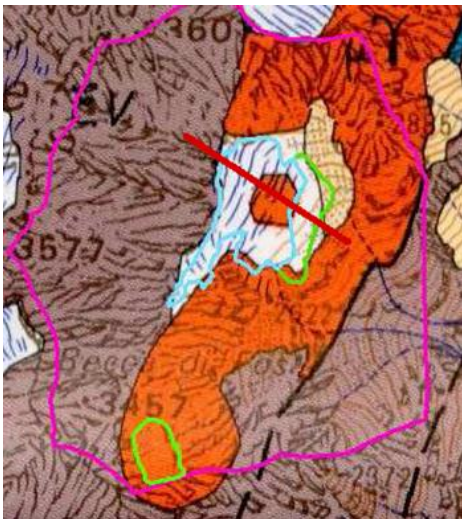


1
 2 **Fig. 1** Small sketch with location of the Aosta Valley Region and detailed layout plan of the Pellaud basin.
 3

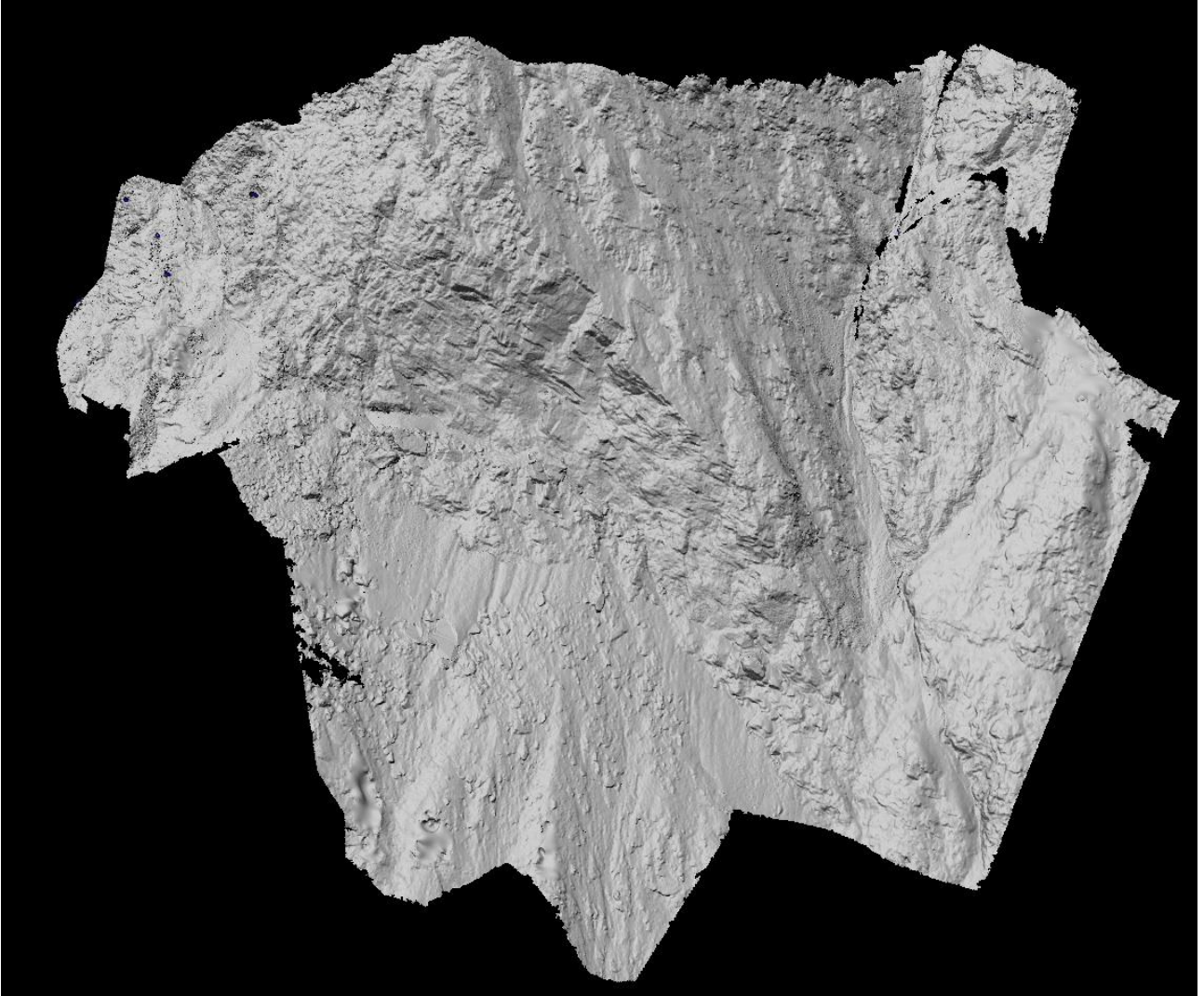


1
2
3
4

Fig. 2 Description of the study area. Area 1: rock debris on the orographical left side of the Pellaud Torrent; Area 2: rock debris on the orographical right side of the Pellaud Torrent

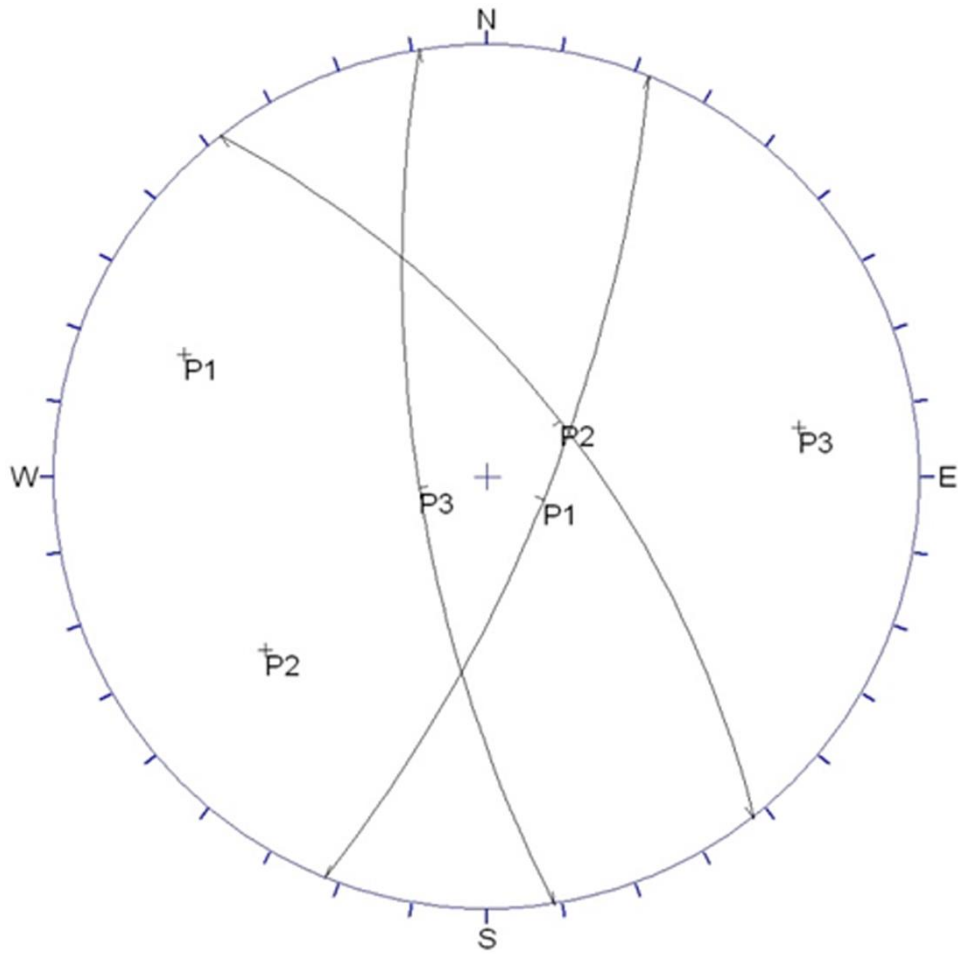


5
6



1

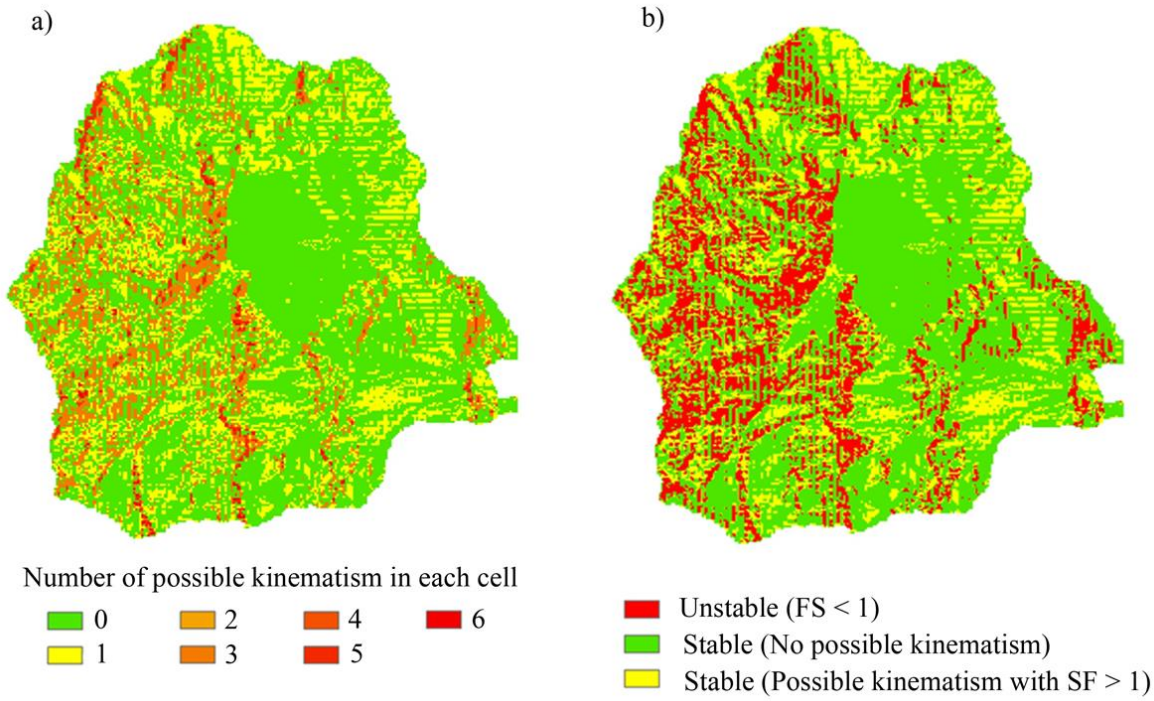
2 **Fig. 3** DSM 3D representation of the Pelaud basin (this area corresponds to that one delimited with pink line in Figure 2).



	System P_i			Intersection R_{ij}		
	P1	P2	P3	R12	R13	R23
Dip [°]	74	66	72	66	42	32
Dip Dir [°]	112	052	261	060	186	339

Fig. 4 Stereographic projection and orientation angles of discontinuity systems.

1
2
3
4
5
6
7
8
9
10
11



1
2
3
4
5
6
7

Fig. 5

Thematic maps of kinematism and instability zones: a) detachment propensity index, proportional to the number of different kinematisms identified in each cell (variable between 0-absence of failure possibility, to 6, co-presence of 6 different failure modes); b) Factor of safety obtained in each cell from the stability analyses carried out considering the different failure mode (results obtained with $\phi=35^\circ$ and zero cohesion).

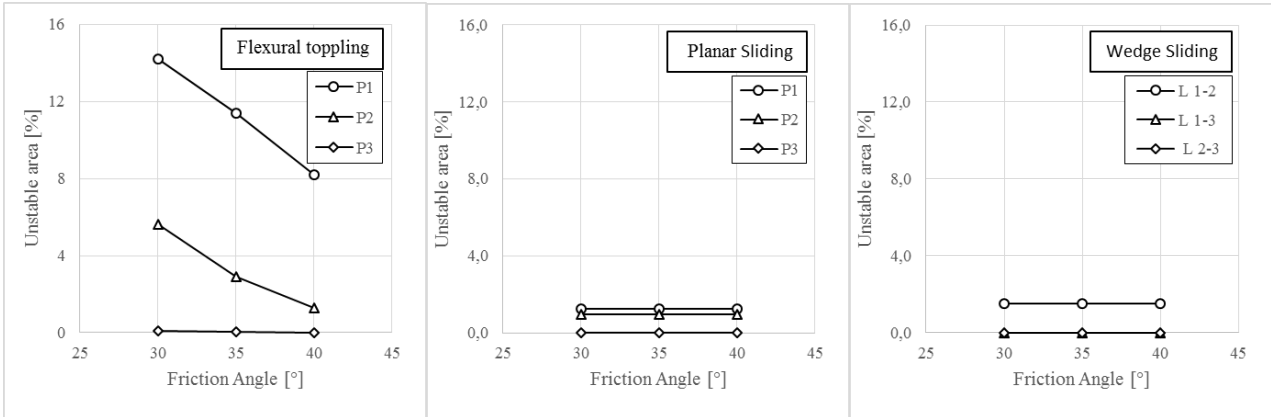
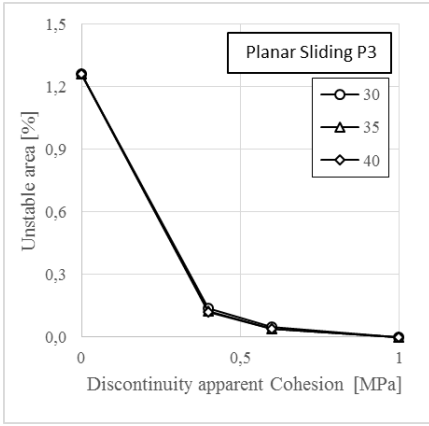


Fig. 6 Unstable area vs. friction angle obtained for flexural toppling, planar sliding and wedge sliding failure mode along the different discontinuity planes and their intersections.

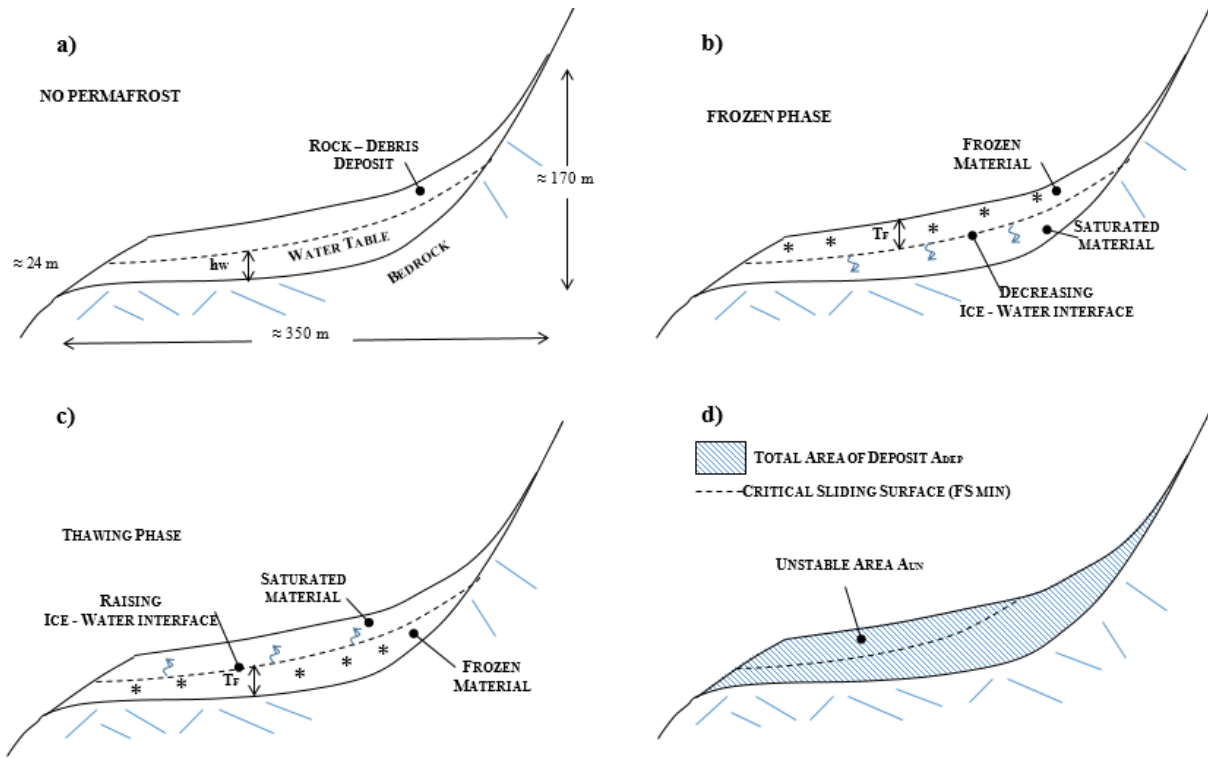
1
2
3
4



1
2
3
4

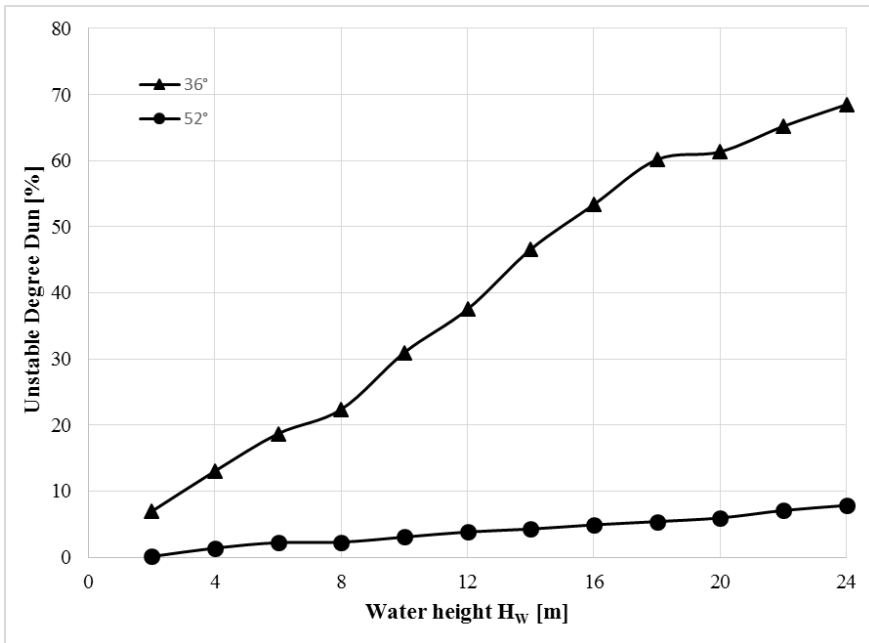
Fig. 7 Unstable area vs. apparent cohesion obtained for sliding along plane P1 by varying the value of discontinuity friction angle.

1

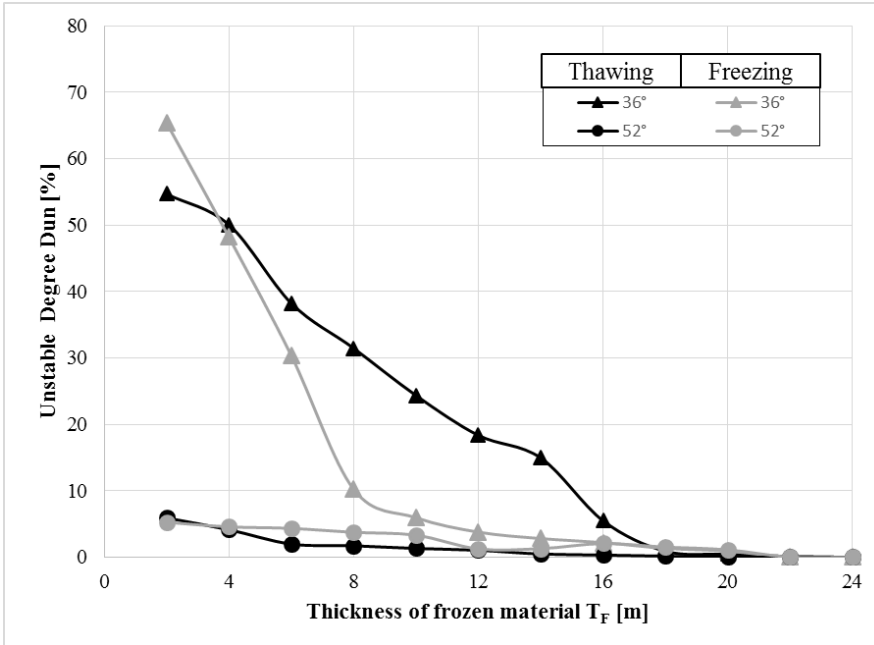


2 **Fig. 8** Not scaled sketch of the analysed section reporting the geometrical setting: a) No-permafrost analyses; b) Freezing
3 phase analyses; c) Thawing phase analyses; d) evaluation of the unstable slope degree D_{UN}

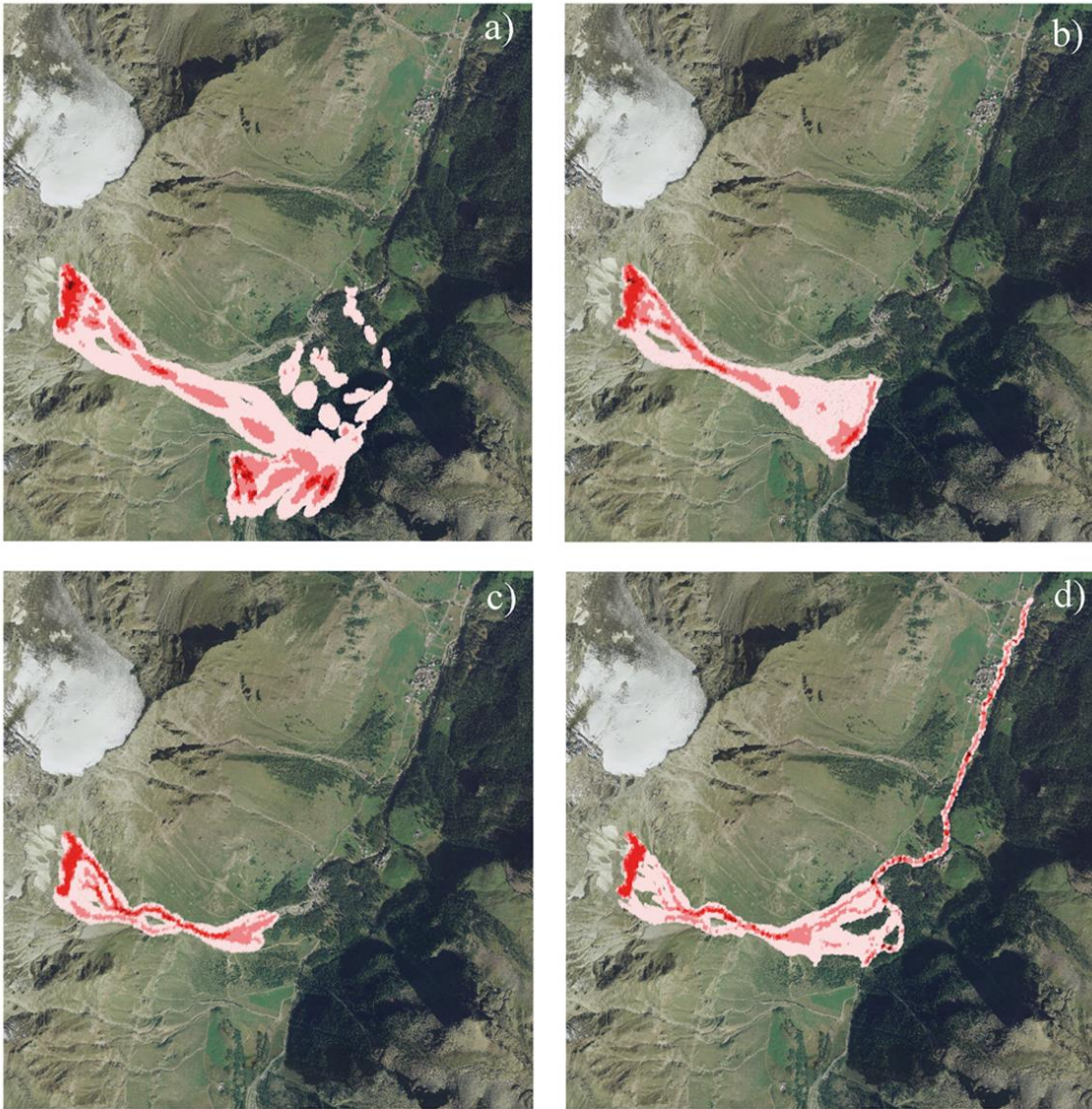
4



1
 2 **Fig. 9** Water height (H_w) vs. unstable Degree (D_{UN}) obtained from no-frozen analyses considering the two limits values
 3 of debris strength parameters.
 4



1
 2 **Fig. 10** Thickness of frozen material (T_F) vs. unstable Degree (D_{UN}) obtained from thaw-freezing analyses considering
 3 the two limits values of debris strength parameters.
 4



1

2 **Fig.11** Scenario A1. Results of the numerical analyses carried out with the RASH^{3D} code. Frictional rheology: a) $\phi = 15^\circ$, b) $\phi = 25^\circ$.

3 Voellmy rheology: c) $\mu=0.1$ - $\xi = 500\text{m/s}^2$, d) $\mu=0.05$ - $\xi = 1000\text{m/s}^2$.

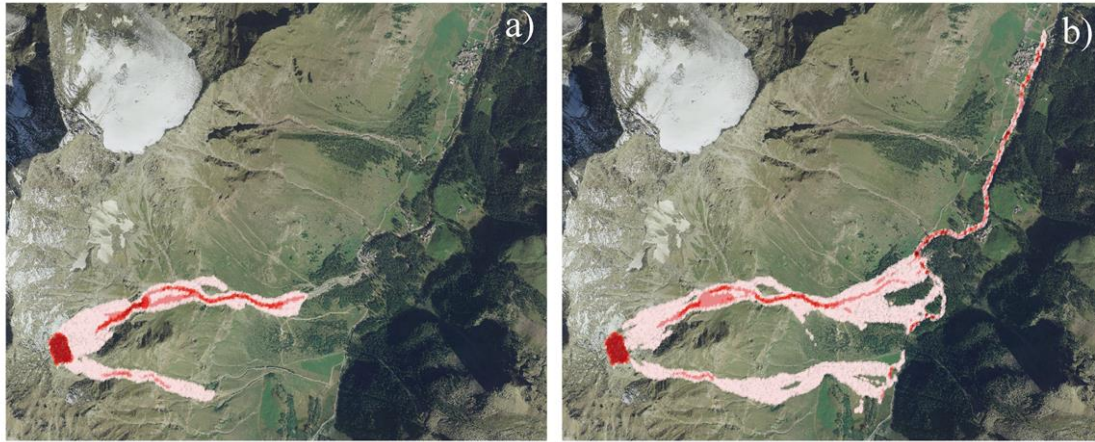
4



1
2
3
4

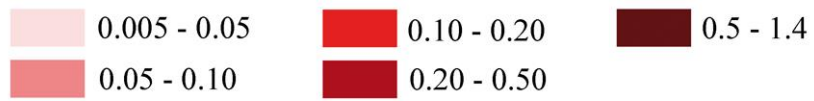
Fig. 12 Details of the Pellaud channel. Arrows indicate the presence of rock blocks deposited during past events. The contour interval is 20 m.

1



Legend

Maximum run-out flow depths [m]:



2

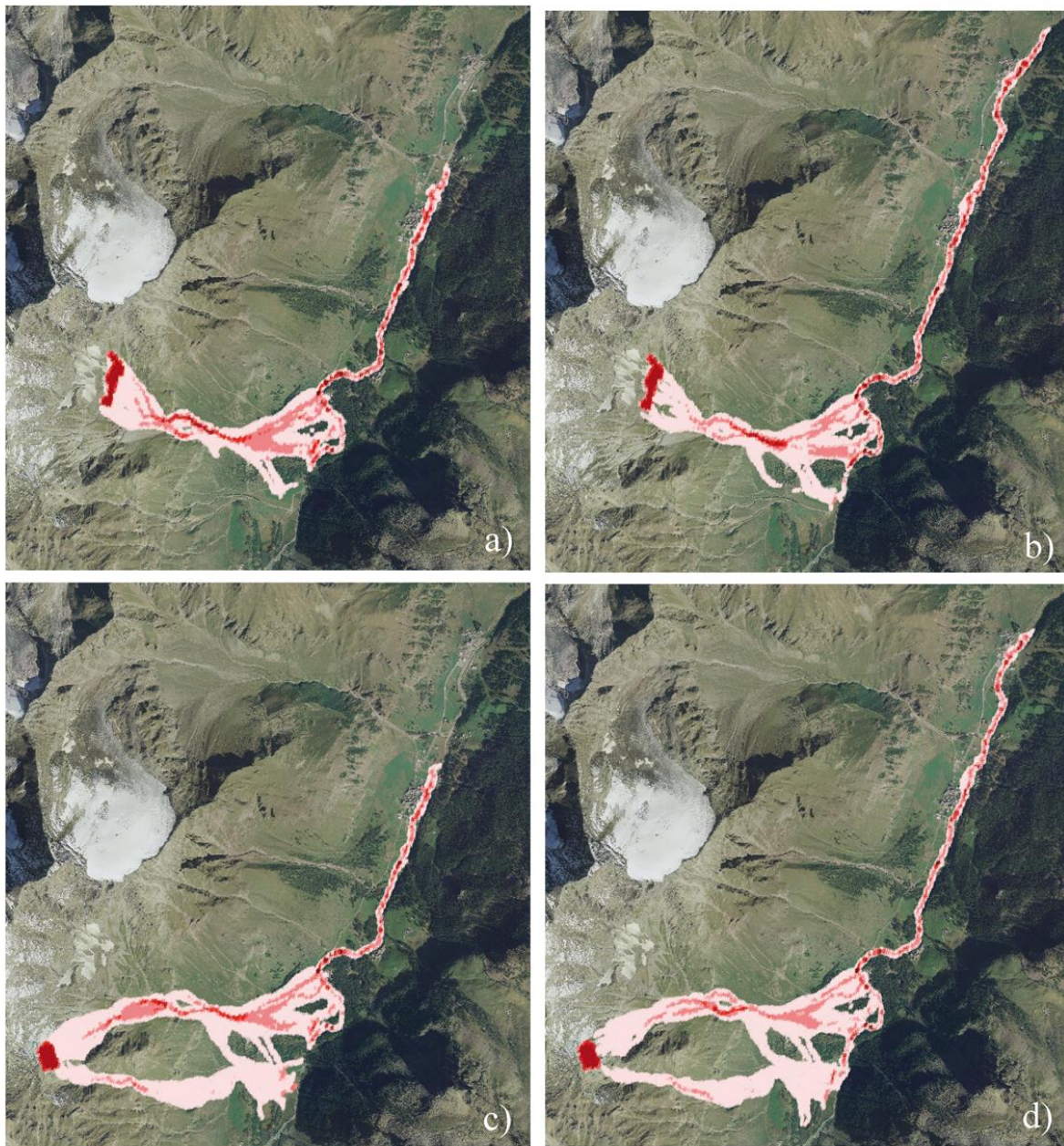
3

Fig. 13 Scenario B1. Results of the numerical analyses carried out with the RASH^{3D} code. Voellmy rheology: a) $\mu=0.1$ - $\xi = 500\text{m/s}^2$,

4

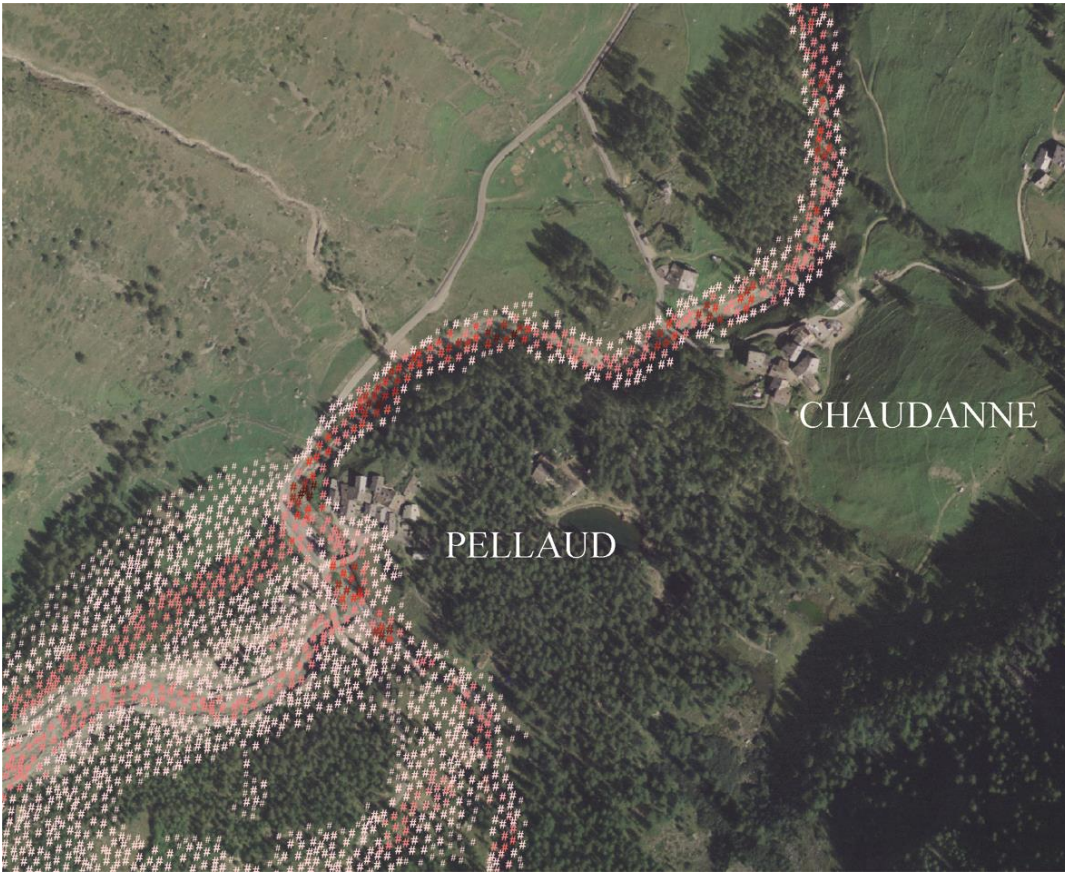
b) $\mu=0.05$ - $\xi = 1000\text{m/s}^2$.

5



1
 2 **Fig. 14** Results of the numerical analyses carried out with the RASH^{3D} code. Scenario A2 - Voellmy rheology: a) $\mu=0.1$ - $\xi = 500\text{m/s}^2$,
 3 b) $\mu=0.05$ - $\xi = 1000\text{m/s}^2$.Scenario B2 - Voellmy rheology: c) $\mu=0.1$ - $\xi = 500\text{m/s}^2$, d) $\mu=0.05$ - $\xi = 1000\text{m/s}^2$.
 4

1



2

3

4

Fig. 15 Involvement of the Pellaud and Chaudanne hamlets in the run-out of the moving mass as obtained by numerical analyses.